Journal of the Korean Ceramic Society
Vol. 49, No. 1, pp. 48~55, 2012.

http://dx.doi.org/10.4191/kcers.2012.49.1.048

Electric-Field Induced Degradation of Ionic Solids

Jakyu Chun and Han-Ill Yoo†

WCU Hybrid Materials Program, Department of Materials Science and Engineering, Seoul National University, Seoul 151-744, Korea

(Received December 27, 2011; Revised January 6, 2012; Accepted January 9, 2012)

ABSTRACT

Degradation of performance and life time of a functional material or device thereof is induced, to a great extent, by mass transfer in the material that is driven by various thermodynamic forces imposed intentionally or accidentally during its operation or service. The forces are any gradient of intensive thermodynamic variables, component chemical potentials, electrical potential, temperature, stresses, and the like. This paper reviews electric-field induced degradation phenomena in ionic solid compounds including insulation resistance degradation, crystal shift, microstructural alterations, compositional unmixing, and compound decomposition. Their inner workings are also discussed qualitatively.

Key words : Electric field, Degradation, Crystal shift, Microstructure alteration, Kinetic unmixing, Decomposition

1. Introduction

Degradation of performance and life time of functional materials is now attracting a wide attention with the devices thereof ever shrinking in size and their service conditions becoming ever harsher. Examples may include electrolytes, mixed ionic electronic conductors, insulators, thermoelectrics, ferroelectrics and dielectrics, piezoelectrics, electrochromics, to name only a few. For the case of $BaTiO_3$-based multilayer ceramic capacitors (MLCC), for example, their sizes have been reduced to only submicron-thick dielectric layers each consisting of only a few $BaTiO_3$ grains of less than 100 nm diameter in tandem, and hence, its electrical tension easily reaches values greater than 10^4 V/cm in their normal operation or service conditions. Under such a huge electrical driving force condition, the insulation resistances (IR) of MLCC's degrade typically as shown in Fig. 1. One can see that depending on samples the IR drop almost abruptly. Degradation tends to be accelerated as a device gets thinner and smaller because of the driving force getting more and more intense.

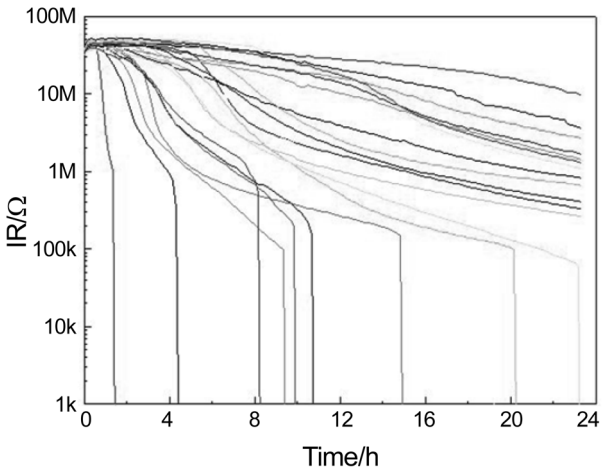

Fig. 1. Degradation of insulation resistances of $BaTiO_3$-based multi-layer ceramic capacitors with time at 120-150°C under ca. 10^4 V/cm, courtesy of Samsung Electro-Mechanics Co., Ltd.

Degradation is, to a great extent, attributed to the mass transfer within and/or across the materials comprising the device, driven by thermodynamic forces imposed intentionally or accidentally during its operation or service. The forces are any gradients of thermodynamic intensive variables of the given material system, component chemical potentials, electrical potential, temperature, stresses, etc. Mass transfer phenomena are typically ionic conduction or electrotransport under electric fields, diffusion or permeation under chemical potential gradients, thermomigration under temperature gradients, creep under stress gradients, etc. The present review is concerned with the degradation phenomena of ionic solids induced by an electric field in particular. The other degradation phenomena will be dealt with in other contributions of this special issue.

Electric field can be applied to a system, in principle, in two ways: one by subjecting the system to an electric field in the open-circuit condition and the other in the closed-circuit condition.[1)] In the former, no current is passed and only charge polarization is expected, but it has been observed[2)] that dislocations and grain boundaries are driven to migrate. No convincing explanations for that, however, are available yet.[1)] In the latter, a current is passed or ionic and electronic transport takes place. This possibly causes chemical reactions or chemical

†Corresponding author : Han-Ill Yoo
E-mail : hiyoo@snu.ac.kr
Tel : +82-2-880-7163 Fax : +82-2-884-1413

polarizations wherever and whenever the divergence of ionic or electronic partial currents does not vanish,[1,3] thus followed by the degradation of function and life time of a functional material.

In this review, we will selectively discuss the electric current-induced degradation phenomena including the IR degradation of dielectrics; crystal shift; microstructural alterations including grain growth, porosity change, contour change and grain boundary migration; compositional unmixing and compound decomposition.

2. IR degradation

The IR degradation of a ferroelectric or dielectric material itself is partially attributed to the electrotransport of ions and electrons under ion-blocking condition imposed by inert metal electrodes.[4] For the case of dielectric $BaTiO_3$, for example, the majority type disorders are, in its virgin state, oxygen vacancies ($V_O^{\bullet\bullet}$) introduced during sintering by doped or background acceptor impurities (A'_C), or $2[V_O^{\bullet\bullet}] \approx [A'_C]$, thus rendering the $BaTiO_3$ matrix electrically insulating. Here [ ] denote the concentration of the thing within them. Once an electric field is imposed, these vacancies are electrotransported to be enriched inward from the cathode and to be depleted inward from the anode, because the metallic electrodes are blocking the ionic current and the lateral boundary of the dielectric normally remains closed with respect to oxygen exchange with the surrounding. Oxygen vacancies enriched over the acceptor level reduce the cathode vicinity to generate electrons (e') to such an extent that $2[V_O^{\bullet\bullet}] \approx n(\equiv [e'])$, thus turning the region to an n-type semiconductor. Oxygen vacancies depleted below the acceptor level oxidize the anode vicinity to generate holes ($h^{\bullet}$) to such an extent that $[A_C'] \approx p(\equiv [h^{\bullet}])$, thus eventually turning the region to a p-type semiconductor. As these two semiconducting regions approach each other with

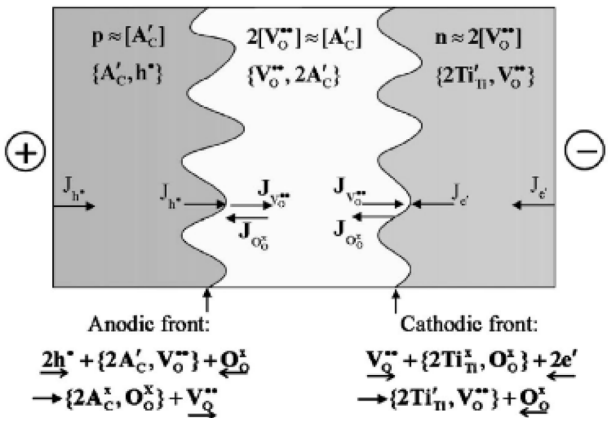

Fig. 2. Electrotransport of oxygen vacancies turns the cathode vicinity to an n-type semiconductor and the anode vicinity to a p-type semiconductor, thus causing the IR of $BaTiO_3$ dielectric to degrade as the two semiconducting regions, $n \approx 2[V_o^{\bullet\bullet}]$ and $p \approx [A'_C]$ expand towards each other with the central insulating region $2[V_o^{\bullet\bullet}] \approx [A'_C]$ shrunken via the reactions at the moving anodic and cathodic front as written. From Ref. 5.

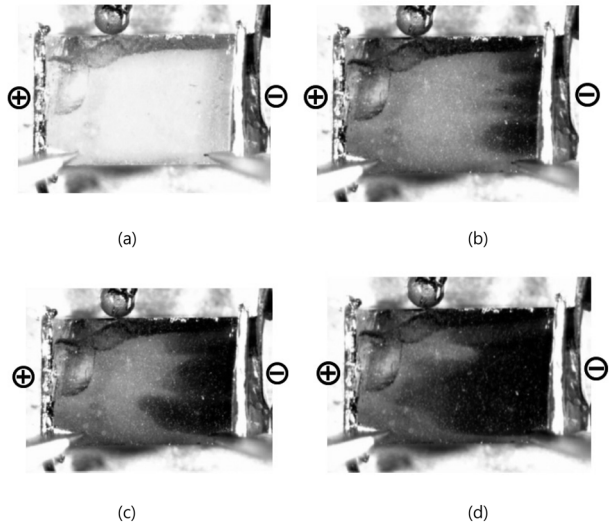

Fig. 3. Color of single crystal $BaTiO_3$ at (a) t = 0, (b) t = 20 s, (c) t = 30 s, and (d) t = 60 s under an electric tension of 45 V/cm at 436°C. Note the cathodic reduced zone in dark color expands toward the anode with time. From Ref. 5.

the central insulating region consequently shrunken, the IR degrades. When the two semiconducting regions finally touch each other, the dielectric material fails completely. The things happening are illustrated in Fig. 2. The growing semiconductor zones are even visible by color changes, see Fig. 3.

3. Crystal Shift

When a mixed ionic electronic conductor oxide $A_{1-\delta}O$ is subjected to an electric field via a pair of reversible gas (O_2) electrodes, the oxide crystal shifts as a whole in the direction of current. An example is shown in Fig. 4: when a current is passed through a disk of CoO via a Pt bead anode and a Pt foil cathode (Fig. 4(a)), the bead anode is rendered to be embedded into the crystal (Fig. 4(b)).

This overall shift may be understood in terms of cation electrotransport and following chemical reaction with gaseous oxygen at the electrodes as illustrated in Fig. 5. Under the action of an electric field, a flux of Co^{2+} cations is initiated at the anode via the reaction,

$$CoO = \frac{1}{2}O_{2(g)} + Co^{2+}(\rightarrow) + 2e^{-}(Pt) \quad (1)$$

and the electrotransported cations react with gaseous oxygen at the cathode via the reverse reaction,

$$\frac{1}{2}O_{2(g)} + Co^{2+}(\rightarrow) + 2e^{-}(Pt) = CoO \quad (2)$$

where e^- denotes the charged component electrons and the arrows indicate the directions of migration in Fig. 5. As a consequence, the existing lattice molecules are annihilated at the anode and the new lattice molecules are generated at the

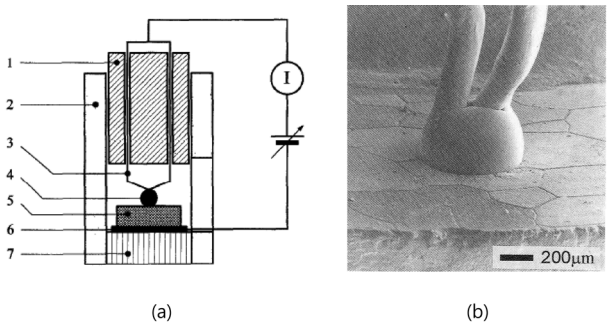

Fig. 4. (a) Experimental setup to demonstrate a crystal shift under an electric field, which is applied to a disk of mixed conductor specimen CoO via a Pt bead anode and a Pt foil cathode, (1: alumina 4-bore tube, 2: alumina tubing, 3: Pt lead wire, 4: bead electrode, 5: specimen, 6: Pt foil electrode, 7: alumina stub) and (b) the bead anode embedded into the crystal afterwards. From Ref. 6.

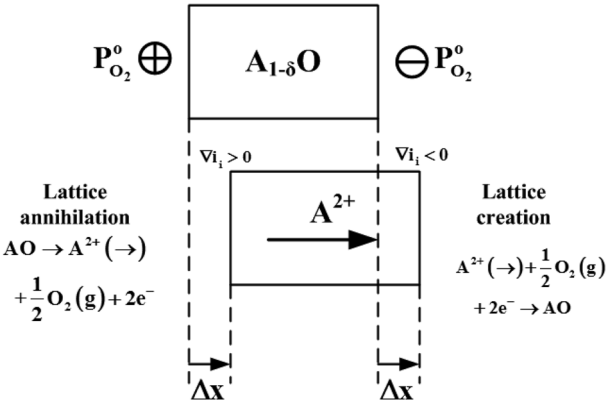

Fig. 5. Electrotransport-induced lattice annihilation and generation at the anode and cathode, respectively, causing the overall crystal to shift in the current direction. Redrawn from Ref. 6.

cathode, causing an overall shift of the crystal in the direction of current. Of course, the anions are also electrotransported in principle, but pass through the crystal without leaving a trace behind if the electrodes are reversible with respect to oxygen exchange. It is emphasized that the flowing cations are all initiated at the anode and stopped completely at the cathode, thus the divergence of the cation current, ∇i_{i+} becomes maximum at the both electrodes, of course, in the opposite sense.

The crystal shift is, therefore, a measure of cation transfer to the total charge transfer, or transference number of cations t_{i+}. Letting ΔV be the volume transported after passing a current I(t) for a time duration t, the ionic transference number may be given for a binary AO as

$$t_{A^{2+}} = \frac{2F(\Delta V/V_{AO})}{\int_0^t I dt} \quad (3)$$

where F is the Faraday constant and V_{AO} the molar volume of AO. One can, thus, take advantage of this degradation

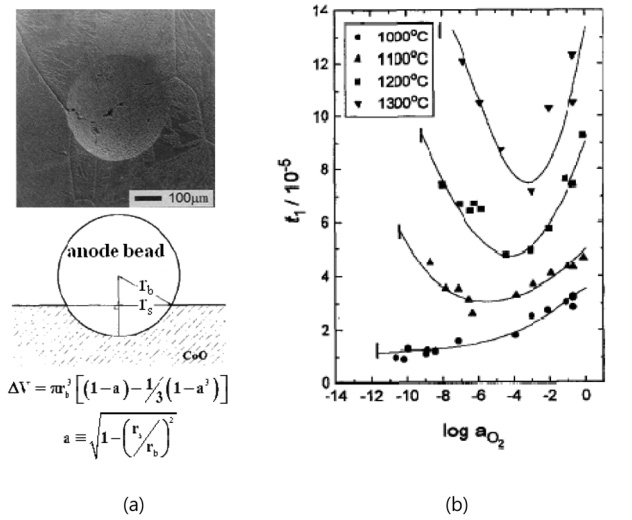

Fig. 6. Electrotransported volume may be determined geometrically as the embedded volume of e.g., a Pt bead anode by using the radius of the bead r_b and of the crater r_s for a total charge transfer given (a), and the resulting cation transference number of CoO as a function of oxygen activity at different temperatures (b). From Ref. 6.

phenomenon to determine the cation transference number of a mixed conductor. An example for AO = CoO is shown in Fig. 6. In this case, the electrotransported volume is measured as the embedded volume of the Pt anode bead shown in Fig. 4(b) for a given charge transfer (Fig. 6(a)), and subsequently the cationic transference number has been determined against oxygen activity at different temperatures due to Eq. (3), see Fig. 6(b).

4. Microstructural Alterations

Whenever and wherever the divergence of the ionic partial current does not vanish or $\nabla i_{i+} \neq 0$, there arises an electrochemical reaction, consequently causing microstructural alterations there, and this normally takes place at the singularities such as heterogeneous phase boundaries, e.g., mixed conductor/metal interfaces and even homogeneous boundaries between a polycrystal and single crystal of the same compound.

Microstructural alterations at the singularities have been demonstrated in an electrotransport cell involving a layer of single crystal CoO sandwiched between two porous polycrystalline pellets of CoO as shown in Fig. 7.[3] After passing a current of 25 A/cm^2 in air atmosphere at 1210°C for 48 h, the sandwich was cut in halves to examine the microstructural changes. Fig. 8 shows the microstructures in the vicinity of the anode (a) and cathode (b). The two are quite contrasted in appearance: The anode side appears no less porous than the original polycrystalline CoO with grains somewhat smaller than the original ones; the cathode side fully dense with much larger grains. Furthermore, a new dense layer of CoO is found to have grown outward passing the row of Pt paste particles together with the Pt net wire which were all located initially

at the polycrystal surface as a part of the cathode, see Fig. 7.

First of all, the outward growth of a new CoO layer across the Pt particles is nothing but a consequence of crystal shift due to the lattice generating reaction Eq. (2). The Pt wire segment, 0.2 mm in diameter, of the Pt net is totally blocking the incoming flow of Co^{2+} cations, thus leaving itself embedded within the newly growing layer.

Next, the densification and grain growth in the vicinity of the cathode is understood to have been started from the interfaces with the cathode Pt particles where the incoming cation flow is completely stopped. Once the flow of the cations is stopped, they react with gaseous oxygen in open pores to fill up the pores by generating the new lattice molecules, thus rendering the porous matrix to become dense and the grains to grow. Subsequently, there arises a difference in the ionic transference number between the original porous matrix and the newly formed dense layer just beneath the cathode. The ionic transference number of the porous matrix must be larger than that in the dense matrix due to the presence of plenty of high diffusivity or ionic conduction paths in the former, thus $\nabla i_{i+} < 0$. The accumulating cations there again react with the gaseous oxygen available in open pores to generate the new lattice molecules. This process perpetuates to make the densification/grain growth propagate inward from the Pt cathode. The result is what is seen to the left of the row of the cathode Pt particles in Fig. 8(b).

Fig. 9 depicts the microstructure around a Pt inner potential probe. Here, one can again see the originally porous matrix has become much denser with grains grown larger only on the left side of the segment of Pt wire inner probe. The phenomenon here is also understood in the same line: cations electrically

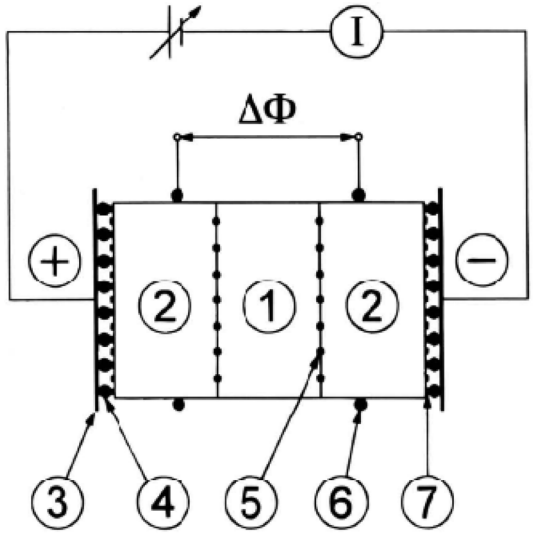

Fig. 7. Configuration of an electrotransport cell involving a sandwich of polycrystal/single crystal/polycrystal CoO equipped with two inner Pt potential probes. (1: single crystal CoO, 2: polycrystalline CoO, 3: Pt foil, 4: Pt mesh electrode, 5, 7: inert Pt markers, 6: inner voltage probes) From Ref. 3.

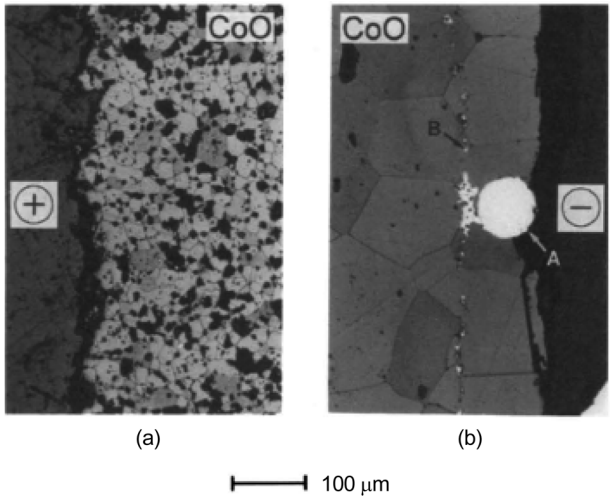

Fig. 8. Microstructures evolved in the vicinity of the anode (a) and the cathode (b) after passing a current of 25 A/cm^2 for 48 h at 1210°C in air atmosphere. From Ref. 3.

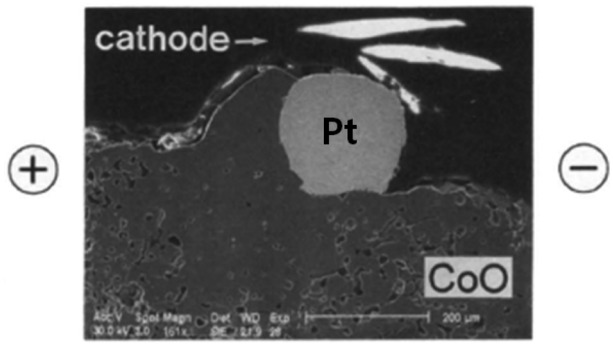

Fig. 9. Microstructure evolved in the vicinity of a Pt wire inner potential probe. Note the densification and grain growth inward from the inner probe and outgrowth of CoO along the surface of the Pt inner probe. From Ref. 3.

driven toward the cathode are blocked by the intervening Pt wire segment, and react with gaseous oxygen available there to generate new oxide lattices molecules outward as well as inward. As the accumulation continues, the outgrowth of the oxide continues along the free surface of the Pt wire segment to alter even the contour of the system, and the densification/grain growth propagates inward from the metal/oxide interface as shown in Fig. 8(b).

Fig. 10 shows a porosity variation across the entire sandwich. As shown, the porosity gradually decreases from the anode up to the interface with the central single crystal and the pattern repeats from the other side of the single crystal through to the cathode. Knowing that the single crystal has smaller value of the cation transference number, one can recognize that there has been an enrichment of Co at the anode-side interface with the single crystal ($\nabla i_{i+} < 0$) and depletion at the other interface ($\nabla i_{i+} > 0$), thus causing the porosity change as observed in Fig. 10. An extreme situation can be realized by replacing the

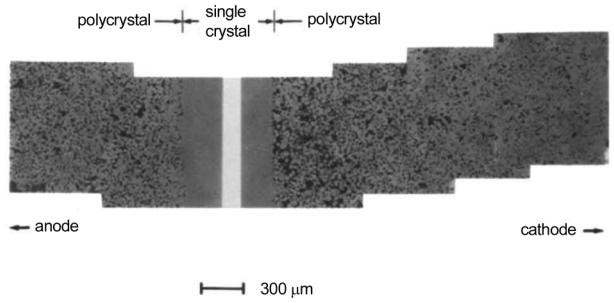

Fig. 10. Electrotransport-induced porosity change across the entire sandwich of the polycrystalline CoO/ single crystal CoO/ polycrystalline CoO after passing a current of 15 A/cm^2 for 120 h at 1100°C in air atmosphere. From Ref. 3.

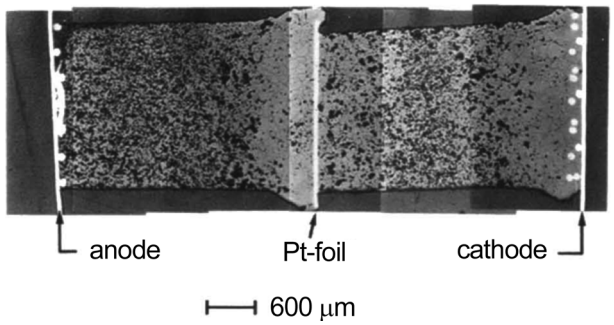

Fig. 11. Panoramic view of the porosity and contour change across the sandwich of porous CoO/Pt-foil/CoO, after passing 20 A/cm^2 for 72 h at 1093°C in air atmosphere. From Ref. 3.

single crystal CoO, which is only a bit less permeable to Co^{2+} cations than the porous CoO, with the totally impermeable Pt-foil in the sandwich. The result is as shown in Fig. 11, which shows the entire panorama of porosity change from the anode through to the cathode. By recognizing that the Pt foil is totally blocking the ionic current, thus, making ∇i_{i+} extreme at its both surfaces, one can more clearly see how densification/ growth propagates in the counter direction to the current and the contour of the system alters.

We have, thus far, seen that wherever $\nabla i_{i+} < 0$, densification and grain growth propagates inward away from there and new lattice molecules form outward. It is then not hard to expect that the single crystal layer itself in the sandwich of polycrystal/single crystal/polycrystal will shift as a whole towards the anode. It is indeed so. Fig. 12 shows the location of polycrystal/single crystal boundaries in the sandwich in Fig. 7 after electrotransport. One can see that the Pt markers, which was initially located at the anode-side surface of the single crystal, remain behind the interface between the newly formed single crystal and original polycrystal at the anode side, and the Pt markers initially located at the cathode-side surface of the single crystal remains there. Obviously, the thickness of the single crystal layer should remain unchanged if and only if $|\nabla i_{i+}|$ is the same at the two interfaces.

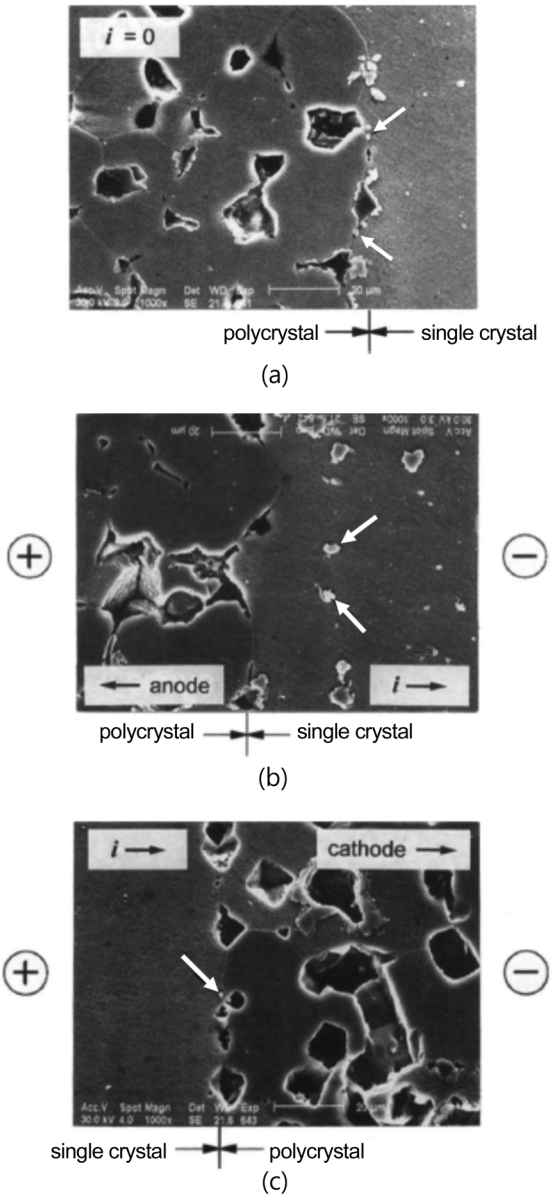

Fig. 12. Locations of the Pt inert markers (marked by the white arrows in the images) after heat treatment at 1100°C for 120 h in air atmosphere (a) without passing a current (i = 0) and (b) with passing a current of 15 A/cm^2 (b, c) through the sandwich of polycrystal CoO/single crystal CoO/polycrystal CoO. Note the growth of a new fully dense layer toward the anode, leaving the markers behind (b) while the markers remain on the polycrystal/single crystal interface on the cathode side (c). From Ref. 3.

5. Kinetic Unmixing

When an ionic solid is ternary or higher in composition, e.g., $(A,B)_{1-\delta}O$, electrotransport induces a further complication in addition to the crystal shift and microstructural alterations discussed so far. Normally different cations have different mobilities by nature, and hence, the fastest moving cations

should tend to be enriched, relative to the slower cations, towards the cathode. This is called kinetic unmixing,[1] which is obviously another critical factor for device degradation.

An example is shown in Fig. 13. Here, a homogeneous ternary ferrite $(Co_xFe_{1-x})_3O_4$ is subjected to an electric field via reversible gas electrodes. Electrotransport has induced Co to be enriched at the cathode in an atmosphere of oxygen partial pressure $p(O_2) = 10^{-6.3}$ atm (Fig. 13(a)) and at the anode in an atmosphere of $p(O_2) = 10^{-2.0}$ atm (Fig. 13(b)). These results indicate that Co cations are faster in the reducing atmosphere, but slower in the oxidizing atmosphere. It is indeed the case as shown in Fig. 14, where the tracer diffusivities of Co and Fe are given against oxygen activity at different temperatures.[8] The unmixing profile under electric field is determined by the difference in the electrochemical mobilities of constituent cations. In the interstitial dominating regime in reducing atmospheres, the electrochemical mobility of Co is larger than that of Fe or $z_{Co}D^*_{Co} < z_{Fe}D^*_{Fe}$ and in the vacancy dominating regime in oxidizing atmospheres, $z_{Co}D^*_{Co} > z_{Fe}D^*_{Fe}$ even though $D^*_{Co} \approx D^*_{Fe}$, where z_k denotes the valence of k-type ions.

As unmixing proceeds to exceed the compositional homogeneity range of a compound, the compound will eventually have to be decomposed into its component compounds, which is termed the kinetic decomposition.[1] It is recently observed[11] from the system of $NiTiO_3$ which has a very narrow range of homogeneity.[9,10] As shown in Fig. 15, electrotransport has induced compositional unmixing across the phase stability range of the ilmenite $NiTiO_3$, but as soon as its stability limits are exceeded, the ilmenite phase has decomposed as indicated by a discontinuous change of the cationic composition.

Decomposition following unmixing is believed to be a quite general phenomenon particularly when a compound has a very narrow range of homogeneity or a line compound, but there is apparently an exception or anomaly. That was observed in the system of 1 mol% La-doped $BaTiO_3$[12] which may be

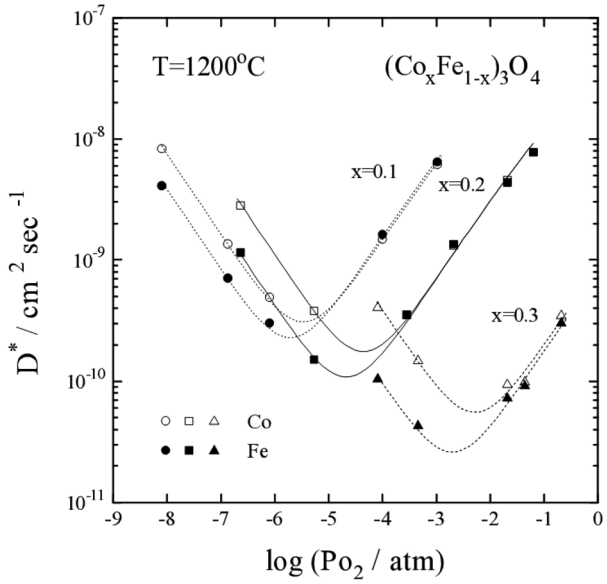

Fig. 14. Tracer diffusivities of Co and Fe vs. oxygen partial pressure for $(Co_xFe_{1-x})_3O_4$, from Ref. 8. Note that $D^*_{Co} > D^*_{Fe}$ in the reducing atmospheres where cation interstitials are in majority, but $D^*_{Co} \approx D^*_{Fe}$ in the oxidizing atmospheres where cation vacancies are in majority.

regarded as a line compound. In this system, it seems to be obvious that Ba and Ti sitting in different sublattices have different electrochemical mobilities. Particularly when doped with La substituting Ba, the charge compensating defects are well known to be Ti-vacancies or $[La^{\bullet}_{Ba}] \approx 4[V'''']_{Ti}$, in air atmosphere at elevated temperatures, thus Ti is expected to have to have much higher a mobility. It had thus been envisaged that the electrotransport would cause Ti^{4+} to be enriched towards the cathode and the perovskite $BaTiO_3$

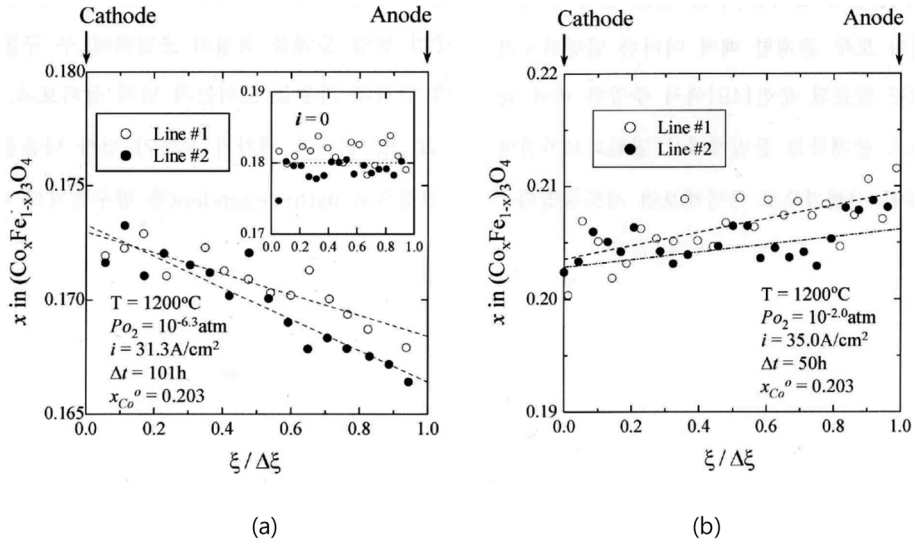

Fig. 13. Electrotransport-induced unmixing of ternary ferrite $(Co_xFe_{1-x})_3O_4$ in a reducing atmosphere (a) and an oxidizing atmosphere (b), from Ref. 7.

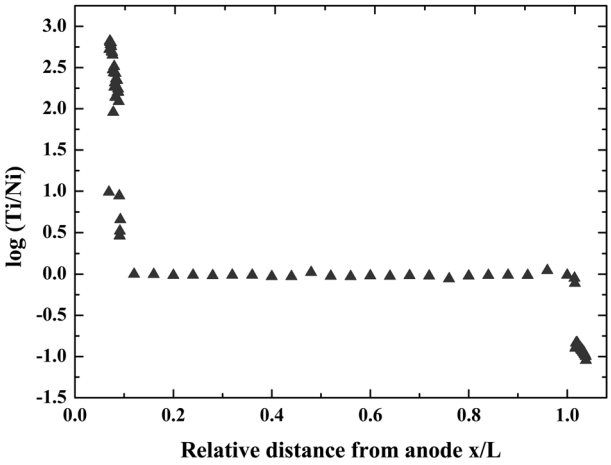

Fig. 15. Electrotransport induces compositional unmixing followed by decomposition of $NiTiO_3$ in the vicinities of the electrodes for the system of $NiTiO_3$ after passing a total charge of 5680 C at 1397°C in air atmosphere. From Ref. 11.

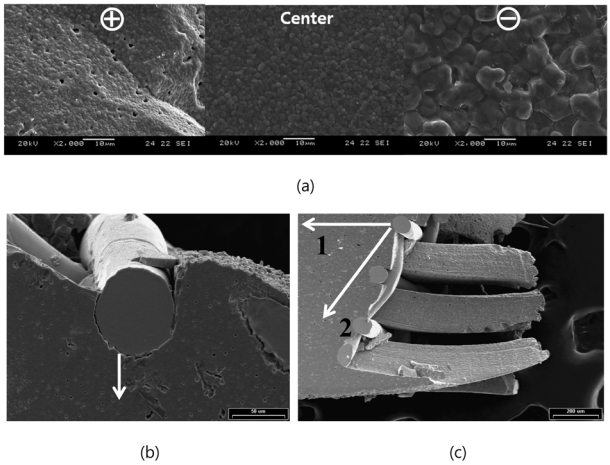

Fig. 16. As-observed microstructural changes across a polycrystalline disk of 1 mole% La-doped $BaTiO_3$ ((a): left, anode portion; center, central portion; right, cathode portion), and in the near vicinities of the cathode (b) and anode (c) after passing a total charge of 1161 C at 1200°C in air atmosphere. From Ref. 12.

phase decompose into a nearest neighboring Ti-excess phase (i.e., $BaTi_3O_7$) at the cathode and a nearest neighboring Ba-excess phase (i.e., Ba_2TiO_4) at the anode.

Fig. 16 shows the microstructural alterations across the specimen of 1 mol % La-doped $BaTiO_3$ from the anode side through the central part to the cathode side (a) and in the near vicinity of the cathode (b) and the anode (c) as observed after passing a charge of 1161 C at 1200°C in air atmosphere. The microstructural changes as observed, including decreasing porosity with increasing grain sizes in the direction of current (in (a)), the Pt cathode being embedded into the newly formed dense oxide (in (b)), and penetration of the Pt anode into the matrix (in (c)) following the annihilation of the existing lattice molecules there, are in general agreement with what we have earlier observed from the system of CoO in Fig. 2. These microstructural changes clearly indicate that there has been electrotransport of cations or mass transfer.

Nevertheless, there has been neither compositional unmixing nor phase decomposition quite contrary to the expectation, as clearly seen in Fig. 17: no unmixed gradients (a) and no decomposition (b) were found within experimental error along the directions indicated by the white arrows in Fig. 16(b) and (c).

Naturally, the simplest guess for the reason is that all the cations should have the same electrochemical mobilities. It may be possible if these three different kinds of cations are electrotransported via an identical vehicle or mechanism, but the same vehicle operating in two different cationic sublattices

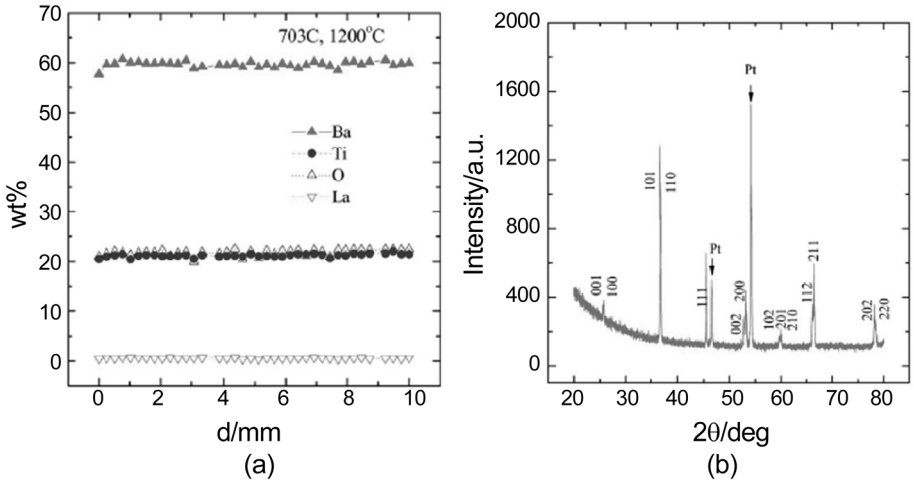

Fig. 17. Concentration distributions of the components Ba, Ti, O and La (a) and x-ray diffraction patterns (b) as examined along the directions indicated by the white arrows in Fig. 16 (b) and (c). Note no composition gradients and no second phase except for perovskite $BaTiO_3$. From Ref. 12.

seems to be not so realistic to conceive. One possibility may then be of a thermodynamic origin: if the compound is a "line" compound with a negligible width of homogeneity range, then the variation of molar Gibbs free energy of the compound vs. composition must be needle-like so that any deviation from the stoichiometric composition should be energetically too costly due to a huge thermodynamic factor (or the restoring force). If this is the case, there can be a mass transfer with no unmixing at all in electric field applied. Obviously, more work and thinking is necessary.

6. Concluding Remarks

We have, thus far, reviewed only a limited number of examples of the current-induced degradation phenomena, the IR degradation, crystal shift, microstructural alterations, kinetic unmixing and decomposition. It seems to be clear that wherever and whenever the divergence of an ionic partial current or flux, whether cationic or anionic, heterogeneous or homogeneous (electro-)chemical reactions then initiate there causing eventually degradation of the performance and lifetime of functional materials and devices thereof. This seems to be general under any other driving force, too. Finding and understanding the correct reasons and mechanisms standing behind a variety of degradation phenomena is crucial for today's technology. However the related works are still extremely limited. Clearly, more systematic works are required on a long term basis.

Acknowledgments

The authors would like to thank the participants in the 1st Workshop on Stability & Degradation of Advanced Materials under Thermodynamic Forces, hosted by the WCU Hybrid Materials Program, Department of Materials Science and Engineering, Seoul National University, Seoul, Korea on April 7-8, 2011 for their sharing of fruitful discussions and the WCU Hybrid Materials Program for her generous financial support for the workshop. This work was supported by the New & Renewable Energy of the Korea Institute of Energy Technology Evaluation and Planning (KETEP) grant funded by the Korea Government Ministry of Knowledge Economy.

REFERENCES

1. H. Schmalzried, Chemical Kinetics of Solids, pp. 183-207, VCH Verlagsgesellschaft, Weinheim, 1995.
2. Z. Munir and H. Schmalzried, "The Effect of External Fields on Mass-Transport and Defect-Related Phenomena," *J. Mater. Synth. Process*, **1** 3-16 (1993).
3. H.-I. Yoo and K.-C. Lee, "Microstructural Changes in a Polycrystalline, Semiconducting Oxide under DC Electric Fields," *J. Electrochem. Soc.*, **145** 4243-47 (1998).
4. R. Waser, T. Baiatu, and K. Haerdtl, "DC Electrical Degradation of Perovskite-type Titanates. I. Ceramics," *J. Am. Ceram. Soc.*, **73** 1645-53 (1990).
5. H.-I. Yoo, M.-W. Chang, T.-S. Oh, C.-E. Lee, and K. D. Becker, "Electrocoloration and Oxygen Vacancy Mobility of $BaTiO_3$," *J. Appl. Phys.*, **102** 093701/1-8 (2007).
6. K.-C. Lee and H.-I. Yoo, "Ionic Transference Number of Semiconducting $Co_{1-\delta}O$," *Solid State Ionics*, **92** 25-36 (1996).
7. J.-O. Hong, Kinetic Demixing of Ternary Ferrite, $(A_xFe_{1-x})_3O_4$ (A=Mn,Co) under an Electric Field (in Korean), pp. 120-21, in Ph. D Thesis, Seoul National University, Seoul, 1999.
8. F.-H. Lu and R. Dieckmann, "Point Defects and Cation Tracer Diffusion in $(Co_xMn_{1-x})_{3-\delta}O_4$ Spinels," *Solid State Ionics*, **67** 145-55 (1993).
9. R. W. Taylor and H. Schmalzried, "The Free Energy of Formation of Some Titanates, Silicates, and Magnesium Aluminate from Measurements Made with Galvanic Cells Involving Solid Electrolytes," *J. Phys. Chem.*, **68** 2444-49 (1964).
10. T. Jacob, V. S. Saji, and S. N. S. Reddy, "Thermodynamic Evidence for Order-Disorder Transition in $NiTiO_3$," *J. Chem. Thermodynamics*, **39** 230-35 (2007).
11. J. Chun, "The Effect of Electric Field on Ternary Oxides," Proc. 8th International Conference on Flow Dynamics, pp. 762-765, Sendai, Japan, 2011.
12. H.-I. Yoo, C.-E. Lee, R. A. de Souza, and M. Martin, "Equal Mobility of Constituent Cations in $BaTiO_3$," *Appl. Phys. Lett.*, **92** 252103/1-3 (2008).